ISBN: 978-3-95450-247-9 ISSN: 2673-5490 doi: 10.18429/JACoW-IPAC2024-WEPG55

LONGITUDINAL PHASE SPACE DENSITY TOMOGRAPHY CONSTRAINED BY THE VLASOV-FOKKER-PLANCK EQUATION

F. Donoso*, S. Funkner, E. Bründermann, M. Reißig, A. Santamaria Garcia, M. Frank, A.-S. Müller,
Karlsruhe Institute of Technology, Karlsruhe, Germany

Abstract

This study introduces a novel approach to longitudinal phase space density tomography in an electron storage ring, using constraints imposed by the Vlasov-Fokker-Planck equation. The Vlasov-Fokker-Planck equation provides a comprehensive description of the evolution of density functions in phase space, accounting for both deterministic and stochastic processes. Measurements of the turn-by-turn bunch profile in electron storage rings offer a time-dependent projection of the phase space. Hence, observing the bunch profile evolution of charged particles in regimes characterised by rich phase space dynamics presents a challenging inverse problem for reconstructing phase space densities.

In this work, we present a tomographic method for reconstructing the longitudinal phase space density of an electron bunch at the Karlsruhe Research Accelerator (KARA). This method utilizes simulated data and applies the Vlasov-Fokker-Planck equation to drive the reconstruction process.

INTRODUCTION

In electron accelerators, understanding longitudinal phase space density's crucial role in accelerator performance sets the stage for the Vlasov-Fokker-Planck equation (VFPE), which effectively models electron beam density evolution by merging electron dynamics under electromagnetic fields with stochastic interactions from the Fokker-Planck equation.

Solving the VFPE for simulating the bunch longitudinal phase space evolution helps in understanding instabilities caused by factors like beam-beam interactions, wakefield effects, and micro-bunching instabilities. Conversely, phase space density tomography is the inverse problem which is mainly used as an diagnostic tool. It involves reconstructing the distribution of particles in phase space based on measured data. This approach is critical for understanding the real dynamics of a beam.

The work of [1] has proved that the longitudinal phase space density of an electron bunch in synchrotrons can be reconstructed utilizing a collection of bunch profile measurements from a single-shot electro-optical (EO) sampling system [2]. The study relies on the progressive rotation of the phase space during turn-by-turn bunch profile measurements and the simplification of the dynamics by a rigid rotation assumption. Considering this, tomography of the phase space density is comparable to a patient rotation in a static CT scanner [3]. Therefore, out-of-the-box tomography methods, for example Filter Back Projection (FBP), can be used for phase-space reconstruction when the phase space remains constant for at least half of the synchrotron oscillation period. However, this approach may encounter challenges when the phase space deforms within each rotation, potentially resulting in significant distortions or inaccuracies in the reconstructed phase space density from the input sequence of measurements.

Phase space density tomography including individual particle dynamics has been developed by [3–8]. The seminal work of Hancock presented a hybrid tomography method which incorporates particle tracking to the well know Algebraic Reconstruction Techniques (ART) [9]. Although phase space density tomography has demonstrated its utility in proton accelerators, its application in electron accelerators encounters limitations. This is primarily due to the inadequacy of particle tracking methods to accurately characterize the self-interaction within the electron distribution, crucial for understanding the dynamics of electron bunches. This becomes apparent, for example, in low momentum compaction operation mode, where micro-bunching instabilities can be observed. Furthermore, tracking macro particles to reduce complexity results in uneven spatial representation, with some regions densely populated and others sparse, leading to high shot noise, thus affecting the accuracy of density calculations [10].

The development of longitudinal phase space density tomography methods specifically designed for electron accelerators is fundamental to study and control the complex dynamics of electron bunches, particularly in accelerators such as fourth generation light sources, where the stability of the beam is key to achieve brilliant photon beams.

PROBLEM STATEMENT

The phase space reconstruction problem can be approached as a partial differential equation constrained optimization problem as in Eq. 1, where the goal is to minimize the error between bunch profile measurements, $\bar{\rho}_n$, and phase space projections, $\rho(q, t_n)$. The objective function is defined by the total distance between measured bunch profiles, and their respective phase space density projections.

$$\begin{aligned} \min_{\psi^*} \quad & \sum_{n=1}^{m} \|\rho(q,t_n) - \bar{\rho}_n\|^2 + \lambda R(\psi) \\ \text{s.t.} \quad & \frac{\partial \psi}{\partial t} + \frac{\partial H}{\partial p}\frac{\partial \psi}{\partial q} - \frac{\partial H}{\partial q}\frac{\partial \psi}{\partial p} = \beta_d \frac{\partial}{\partial p}(p\psi) + D\frac{\partial^2 \psi}{\partial p^2}, \\ & \psi(q,p,t_1) = \psi^*, \end{aligned} \tag{1}$$

where ψ is the phase space density, m is the number of measurements, H is the Hamiltonian of the system, β_d and D

* felipe.donoso@kit.edu

ISBN: 978-3-95450-247-9 ISSN: 2673-5490 doi: 10.18429/JACoW-IPAC2024-WEPG55

are the damping and drift parameters, and q and p are the canonical coordinates position and momentum, respectively. The phase space density projection is determined by integrating along the momentum axis. The incorporation of regularization terms $\lambda R(\psi)$, plays a crucial role in mitigating challenges such as noise in measurement data and the ill-posed nature of the inverse problem.

The solution of the VFPE gives the temporal evolution of the density function. This essentially correlates the phase space density at a given time, $\psi(q,p,t)$, with the next phase space $\psi(q,p,t+\Delta t)$, for a small Δt. To simplify the algorithm, the minimization aims to determine the initial phase space density, ψ^*, from a sequence of bunch profile measurements.

PHASE SPACE DENSITY TOMOGRAPHY

This research uses the numerical solver Inovesa, a VPFE solver developed at KIT [11]. This software is based on the work of Warnock and Ellison [12], which simplifies and solves the VFPE through operator-splitting into three operators. The "rotation" (R) and "wake potential" (K) operators are derived from the Vlasov part of the equation through the application of the Liouville theorem, while the "damping and diffusion" (D) operator comes from the Fokker-Planck terms through numerical differentiation

$$\psi(q,p,t+\Delta t) \approx \mathrm{D} \circ \mathrm{R} \circ \mathrm{K}(\rho(t)) \circ \psi(q,p,t). \quad (2)$$

Operators in Eq. 2 may not be linear. The method in this work linearizes the operators into matrix form using Lagrange Polynomial interpolation.

Operators R and K arise from Liouville's theorem applied to the Vlasov equation, ensuring density conservation along particle paths, as shown in Eq. 3 for a discretized phase space, where x' and y' are founded by the inverse dynamics of the particle.

$$\psi(x,y,t+\Delta t) = \psi(x',y',t). \quad (3)$$

The bi-cubic Lagrange polynomial interpolation for the x' and y' is:

$$\psi(x,y,t+\Delta t) \approx \sum_k \sum_h \psi(x_k,y_h,t) L_h(y') L_k(x'), \quad (4)$$

where $\psi(x_k,y_h,t)$ are prior known density values on the discrete phase space, with k and h spanning over four close nodes on the x and y axis, respectively. $L_k(x')$ and $L_h(y')$ are the Lagrange polynomials at coordinates set by inverse dynamics. This bi-cubic interpolation approach allows for axis-wise interpolation without inter-axis correlation, thus independent operators per axis.

To allow for matrix operator representation, the discrete phase space is expressed as a vector. The new one-dimensional coordinate s is defined as follows:

$$s := N \times x + y + 1, \quad (5)$$

where x and y are the discrete coordinates within the square phase space grid, and N is the length of its side. The interpolation in one axis can be expressed in terms of s as:

$$\psi(s_i,t+\Delta t) = \sum_j \psi(s_j,t) L_j(r_i'). \quad (6)$$

Here r_i' is the continuous one-dimension coordinate corresponding to the inverse particle dynamic: x' or y'.

Eq. 6 can be expressed as a transition matrix, L, for all instances of s. The weights of matrix L depend on the Lagrange polynomials at the interpolated continuous coordinate r_i'. Matrix L correspond to the interpolation in one axis, with 4 nodes points, cubic interpolation, per interpolation (row) of the matrix. Multiplying two matrices for different coordinates yields a matrix with 16 coefficients, characteristic of bi-cubic interpolation.

The operator D is calculated by approximating the first and second derivatives of phase space to momentum, as shown in Eq. 7, using the derivatives of the Lagrange polynomials [13].

$$\begin{aligned} \frac{\partial\psi}{\partial t} &= \beta_d \frac{\partial}{\partial p}(p\psi) + D\frac{\partial^2\psi}{\partial p^2}, \\ \psi(q,p,t+\Delta t) &= \frac{\partial\psi}{\partial t}\Delta t + \psi(q,p,t). \end{aligned} \quad (7)$$

The matrix notation for the presented operators over the phase space is expressed as:

$$\psi(s,t+\Delta t) = \mathrm{L} \cdot \psi(s,t). \quad (8)$$

The evolution of phase space density is expressed in terms of the matrix operators as follows:

$$\psi(s,t+\Delta t) = \mathrm{D} \cdot \mathrm{R_K} \cdot \mathrm{R_D} \cdot \mathrm{K}(\rho(t)) \cdot \psi(s,t). \quad (9)$$

The operator R is divided into the drift operator $\mathrm{R_D}$ and the RF kick operator $\mathrm{R_K}$ for axis-specific application. The transformation M for brief intervals Δt is defined as:

$$\mathrm{M}(\rho(t)) = \mathrm{D} \cdot \mathrm{R_K} \cdot \mathrm{R_D} \cdot \mathrm{K}(\rho(t)), \quad (10)$$

furthermore

$$\psi(s,t+\Delta t) = \mathrm{M}(\rho(t)) \cdot \psi(s,t). \quad (11)$$

Note that although the operator matrices start sparse, matrix M becomes densely populated over iterations. The transfer matrices D, $\mathrm{R_K}$, and $\mathrm{R_D}$ stay constant, but the wake field transfer matrix changes with the bunch profile at a time t.

The bunch profile corresponds to a projection to the q-axis of the phase space density. At time $t+\Delta t$ the relation is as follows:

$$\rho(q,t+\Delta t) = \int \psi(q,p,t+\Delta t)\mathrm{d}p. \quad (12)$$

Equation 12 can be expressed in discrete terms utilizing a projection matrix, W, as follows:

$$\rho(x,t+\Delta t) = \mathrm{W} \cdot \psi(s,t+\Delta t). \quad (13)$$

ISBN: 978-3-95450-247-9 ISSN: 2673-5490 doi: 10.18429/JACoW-IPAC2024-WEPG55

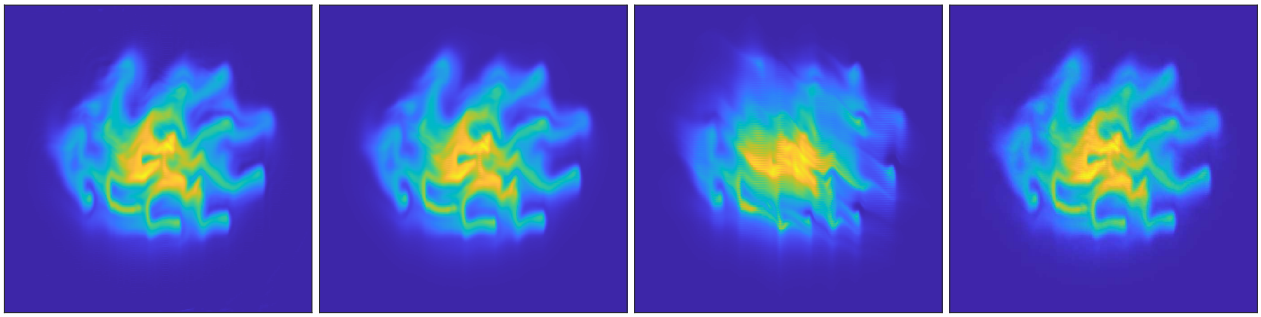

(a) (b) (c) (d)

Figure 1: (a) Target phase space. (b)Method: `IRconstr_ls`, m: 164, RMS: 3.8e−04. (c) Method: `IRnnfcgls`, m: 64 first sequence, RMS:3.1e−03. (d) Method: `IRnnfcgls`, m: 64 random from half synchrotron period, RMS: 5.1e−04.

Subsequently, by substituting Eq. 11 into Eq. 13, the latter can be expressed as:

$$\rho(x, t + \Delta t) = \mathrm{W} \cdot \mathrm{M}(\rho(t)) \cdot \psi(s, t). \tag{14}$$

Equation 14 not only correlates a specific phase space with the next bunch profile but also links it to future profiles. With m bunch profile measurements, the relationship to the initial phase space density is as follows:

$$\begin{aligned} \mathrm{W} \cdot \psi_1 &= \bar{\rho}_1 \\ \mathrm{W} \cdot \mathrm{M}(\bar{\rho}_1) \cdot \psi_1 &= \bar{\rho}_2 \\ \mathrm{W} \cdot \mathrm{M}(\bar{\rho}_2) \cdot \mathrm{M}(\bar{\rho}_1) \cdot \psi_1 &= \bar{\rho}_3 \\ &\vdots \\ \mathrm{W} \cdot \mathrm{M}(\bar{\rho}_{m-1}) \cdots \mathrm{M}(\bar{\rho}_1) \cdot \psi_1 &= \bar{\rho}_m \end{aligned} \tag{15}$$

In order to improve readability the variables in ψ and $\bar{\rho}$ have been omitted and substituted only by a sub-index denoting time. The first equation links the initial bunch profile measured $\bar{\rho}_1$ and its phase space density ψ_1 via the projection matrix W. The next equation ties the second bunch profile $\bar{\rho}_2$ to ψ_1, using both the transfer matrix $\mathrm{M}(\bar{\rho}_1)$ and W. Subsequent equations have a comparable structure, allowing Eq. 15 to be represented in condensed matrix form as:

$$\tilde{\mathrm{W}} \cdot \psi = \rho, \tag{16}$$

where $\tilde{\mathrm{W}}$ is the dynamic projection matrix constructed alongside the arrival of bunch profile measurements, ψ denotes the target phase space density as a vector, and ρ represents the vector-form bunch profile measurements.

Employing the methodology delineated in this section, the inverse challenge of reconstructing phase space density, as shown in Eq. 1, can be reformulated as follows:

$$\min_{\psi} \quad \|\tilde{\mathrm{W}}\psi - \rho\|^2 + \lambda R(\psi). \tag{17}$$

Equation 17 presents a classical tomography problem, addressed with established inverse algorithms.

RESULTS

The tomography problem of Eq. 17 was solved using Inovesa-simulated bunch profiles, with a dataset of 164 measurements spanning half a synchrotron period. To solve Eq. 17, we employed algorithms from the "IR Tools" Matlab library [14], testing 15 algorithms and different subset of sampling measurements, chosen either sequentially or randomly from the 164 bunch profiles.

RMS errors were determined through a comparative analysis between the simulated phase space density, Fig. 1(a), and outcomes derived from every algorithmic combination, utilizing simulated bunch profiles as inputs.

The lowest error was achieved with `IRconstr_ls` (Fig. 1(b), a method using 164 bunch profiles with projected-restarted constraints optimization method [14]. For trials with a subset of 64 bunch profiles, `IRnnfcgls` proved most effective, employing a flexible CGLS (Krylov subspaces) approach for non-negative constraints [15]. Randomly selected measurement subsets outperformed sequential selections, as they cover a 180-degree rotation, whereas sequential selections sample less than 90 degrees. These results are illustrated in Figures 1(c) and 1(d). It is important to notice that `IRnnfcgls` is three times faster than `IRconstr_ls` and thirty times faster that `IRart` (ART method), consistently across all scenarios.

CONCLUSION

The algorithm introduced in this study demonstrates remarkable accuracy and adaptability for reconstructing longitudinal phase space density. Future endeavors may apply this algorithm to empirical data collected through the electro-optical system at KARA.

A parallel computing-based efficient implementation is planned to expedite the construction of the dynamic projection matrix, $\hat{W}$, recognized as the algorithm's most computationally demanding component.

ACKNOWLEDGEMENTS

Gratitude to MathSEE PhD bridge program at KIT, and to P. Schönfeldt for valuable discussions on Inovesa.

REFERENCES

[1] S. Funkner *et al.*, "Revealing the dynamics of ultrarelativistic non-equilibrium many-electron systems with phase space

ISBN: 978-3-95450-247-9 ISSN: 2673-5490 doi: 10.18429/JACoW-IPAC2024-WEPG55

tomography," *Scientific Reports*, vol. 13, no. 1, p. 4618, 21, 2023. doi:10.1038/s41598-023-31196-5

[2] L. Rota *et al.*, "KALYPSO: Linear array detector for high-repetition rate and real-time beam diagnostics," *Nuclear Instruments and Methods in Physics Research Section A: Accelerators, Spectrometers, Detectors and Associated Equipment*, vol. 936, pp. 10–13, 2019. doi:10.1016/j.nima.2018.10.093

[3] S. Hancock, M. Lindroos, E. McIntosh, and M. Metcalf, "Tomographic measurements of longitudinal phase space density," *Computer Physics Communications*, vol. 118, no. 1, pp. 61–70, 1, 1999. doi:10.1016/S0010-4655(99)00194-0

[4] S. Hancock, A. Jansson, and M. Lindroos, "Tomographic Reconstruction of Transverse Phase Space from Turn-by-Turn Profile Data," in *Proc. PAC'99*, New York, NY, USA, Mar. 1999, pp. 2226–2228. https://jacow.org/p99/papers/WEA155.pdf

[5] S. Hancock, M. Lindroos, and S. Koscielniak, "Longitudinal phase space tomography with space charge," *Physical Review Special Topics - Accelerators and Beams*, vol. 3, no. 12, p. 124 202, 12, 2000. doi:10.1103/PhysRevSTAB.3.124202

[6] S. Hancock and J. Sanchez, "A pedestrian guide to online phase space tomography in the CERN PS complex," PS/RF/Note 2001-010, 2001.

[7] C. Grindheim and S. Albright, "Longitudinal Phase Space Tomography Version 3," CERN-ACC-NOTE-2021-0004, 2021.

[8] S. C. P. Albright, C. H. Grindheim, A. Lasheen, and A. H. C. Lu, "Recent Developments in Longitudinal Phase Space Tomography," in *Proc. IPAC'22*, Bangkok, Thailand, 2022, pp. 347–350. doi:10.18429/JACoW-IPAC2022-MOPOPT043

[9] R. Gordon, "A tutorial on art (algebraic reconstruction techniques)," *IEEE Transactions on Nuclear Science*, vol. 21, no. 3, pp. 78–93, 1974. doi:10.1109/TNS.1974.6499238

[10] P. Kuske, "Calculation of Longitudinal Instability Threshold Currents for Single Bunches," in *Proc. ICAP'12*, Rostock-Warnemunde, Germany, Aug. 2012, pp. 267–269. https://jacow.org/ICAP2012/papers/THSDC3.pdf

[11] P. Schönfeldt, M. Brosi, M. Schwarz, J. L. Steinmann, and A.-S. Müller, "Parallelized Vlasov-Fokker-Planck solver for desktop personal computers," *Physical Review Accelerators and Beams*, vol. 20, no. 3, p. 030 704, 14, 2017. doi:10.1103/PhysRevAccelBeams.20.030704

[12] R. L. Warnock and J. A. Ellison, "A General Method for Propagation of the Phase Space Distribution, with Application to the Sawtooth Instability," 2000. doi:10.2172/753322

[13] L. Nguyen, "An extension of Lagrange interpolation to approximate derivative, integral and bivariate function," Open Science Framework, preprint, 12, 2021. doi:10.31219/osf.io/tn67p

[14] S. Gazzola, P. C. Hansen, and J. G. Nagy, "IR Tools: A MATLAB package of iterative regularization methods and large-scale test problems," *Numerical Algorithms*, vol. 81, no. 3, pp. 773–811, 2019. doi:10.1007/s11075-018-0570-7

[15] S. Gazzola and Y. Wiaux, "Fast Nonnegative Least Squares Through Flexible Krylov Subspaces," *SIAM Journal on Scientific Computing*, vol. 39, no. 2, A655–A679, 2017. doi:10.1137/15M1048872